

Interactive Hemocompatible Nanocoating to Prevent Surface-Induced Coagulation in Medical Devices

Jonas Quandt, Manuela Garay-Sarmiento, Lena Witzdam, Jenny Englert, Yannik Rutsch, Cornelia Stöcker, Fabian Obstals, Oliver Grottke, and Cesar Rodriguez-Emmenegger*

Interfacing blood with any artificial surface instantly triggers the activation of coagulation at the interface, posing a risk of adverse thromboembolic complications. Immediately upon contact, blood proteins adsorb to the surface turning it into an active prothrombogenic and proinflammatory interface promoting the activation of platelets and the coagulation cascade. Here, an interactive hemocompatible nanocoating is designed that synergistically combines antifouling polymer brushes with the activity of an anti-FXIIa antibody to tackle the two main causes of surface-induced coagulation. The brushes provide a passive layer rendering the surface stealth and non-thrombogenic against blood activation. Furthermore, as soon as traces of FXIIa arise, the coating immediately and specifically scavenges it, thus actively switching-off contact activation right at the beginning. Moreover, a means is developed to translate this coating to a broad range of polymeric surfaces commonly used in medical devices. The coated surfaces prevent protein adsorption and provide a barrier to bacterial colonization while being capable of capturing biologically relevant concentrations of FXIIa. Notably, the coating completely prevents the formation of clots on the surface when exposed to blood. Thus, the interactive anti-FXIIa nanocoating provides a new avenue to improve the hemocompatibility of medical devices in a safe and efficient manner.

is related to the poor compatibility of these surfaces with blood. Surfaces consisting of synthetic polymers such as poly(4-methyl-1-pentene) (PMP), polyethylene (PE), polycaprolactone (PCL), and poly(dimethylsiloxane) (PDMS) have a low surface energy and a concomitantly high interfacial energy with water.^[2] This drives the adsorption of bio-macromolecules, especially proteins onto the surface within seconds after contact with blood.^[2b,3] The adsorption process is accompanied by changes in the conformation, which turn these otherwise innocuous proteins into an active prothrombogenic and proinflammatory interface.^[2a,3f] For example the adsorption of coagulation factor XII (FXII) zymogen leads to the mechanical cleavage of a bond resulting in the formation of α -FXIIa, which is catalytically active to cleave plasma prekallikrein (PPK) to kallikrein (Figure 1A).^[4] The latter, in turn, activates FXII in a positive feedback loop mechanism, which fuels the rapid elevation of FXIIa concentration in the vicinity

1. Introduction

The contact of blood with any artificial surface immediately triggers the activation of coagulation, leading to device-induced thrombosis generating a risk of life-threatening complications.^[1] The cause for the activation of coagulation

of the surface. This subsequently activates the intrinsic coagulatory pathway encompassing several amplification steps that result in clot formation at the surface.^[5] Moreover, the adsorption of fibrinogen, albumin, and von Willebrand factor leads to conformational changes that expose domains to which platelet integrins can bind. This causes platelet activation and secretion of

J. Quandt, M. Garay-Sarmiento, L. Witzdam, J. Englert, Y. Rutsch, C. Stöcker, F. Obstals, C. Rodriguez-Emmenegger
DWI – Leibniz Institute for Interactive Materials
Forckenbeckstraße 50, D-52074 Aachen, Germany
E-mail: rodriguez@dwirwth-aachen.de

J. Quandt, L. Witzdam, Y. Rutsch, F. Obstals
Institute of Technical and Macromolecular Chemistry
RWTH Aachen University
D-52074 Aachen, Germany

 The ORCID identification number(s) for the author(s) of this article can be found under <https://doi.org/10.1002/admi.202201055>.

© 2022 The Authors. Advanced Materials Interfaces published by Wiley-VCH GmbH. This is an open access article under the terms of the Creative Commons Attribution-NonCommercial License, which permits use, distribution and reproduction in any medium, provided the original work is properly cited and is not used for commercial purposes.

M. Garay-Sarmiento, J. Englert
Chair of Biotechnology
RWTH Aachen University
D-52074 Aachen, Germany

O. Grottke
Department of Anesthesiology
RWTH Aachen University Hospital
Pauwelsstraße 30, D-52074 Aachen, Germany

C. Rodriguez-Emmenegger
Institute for Bioengineering of Catalonia (IBEC)
The Barcelona Institute of Science and Technology (BIST)
Carrer de Baldiri Reixac, 10, 12, Barcelona 08028, Spain

C. Rodriguez-Emmenegger
Institutió Catalana de Recerca i Estudis Avançats (ICREA)
Passeig Lluís Companys 23, Barcelona 08010, Spain

DOI: 10.1002/admi.202201055

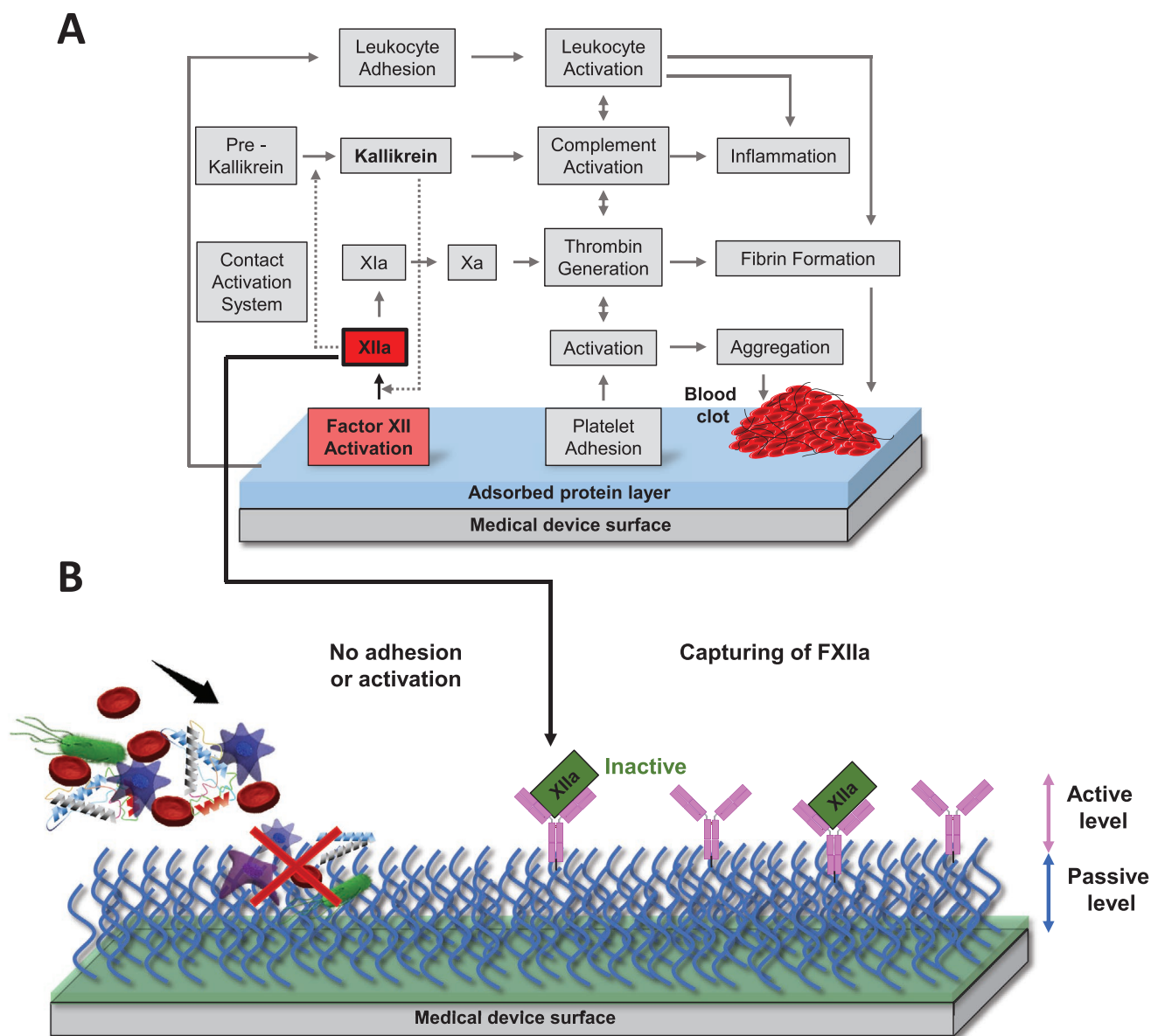


Figure 1. A) Surface-induced activation of blood resulting in coagulation. B) Scheme of the interactive coatings presented herein. Polymer brushes (passive level) provide a stealth interface that prevents the adsorption and unfolding of proteins and is repellent to platelets and other blood cells. Anti-FXIIa is immobilized on top of the brushes (active level) and specifically captures and inactivates FXIIa at the surface.

microvesicles that further activate coagulation at the interface and disseminate away from it.^[6] The presence of these adsorbed proteins or even just nucleophilic groups at surfaces also promotes the adsorption of complement C3b. Even tiny amounts of adsorbed C3b lead to the formation of a surface-bound complex with proteolytic activity.^[7] This complex cleaves circulating complement C3 via the “tick-over” mechanism into more C3b, which adsorbs resulting in more fouling and activation of coagulation and inflammation.^[8] These examples highlight that even minuscule amounts of adsorbed proteins can lead to self-amplifying mechanisms that irretrievably render the surface prothrombotic causing the failure of the device.

Various coatings have been developed to improve the hemocompatibility of surfaces.^[9] They are based on two general concepts: the minimization of protein–surface interactions

to prevent activation (passive coatings) and the modulation of different stages of the coagulation cascade, the inhibition of routes of activation, or reversing clot formation (active coatings).^[10] The former strategy is based on antifouling coatings, which aim at reducing the thermodynamic drive for protein adsorption by minimizing the interfacial energy between the surface and water.^[3e] Such coatings are collectively termed antifouling due to their stealth properties and include self-assembled monolayers, physisorbed (bio)macromolecules, hydrogels, polymer mushrooms, and highly dense end-tethered polymer brushes.^[11] The latter hydrophilizes the surface and introduces enthalpic and entropic barriers, which prevent both penetration and adsorption of proteins and cells.^[12] Poly(ethylene glycol) brushes have been considered the gold standard as they combine hydrophilicity with the high flexibility necessary for the

kinetic barrier.^[12c,13] However, recent studies have shown that some plasma proteins can specifically interact with these coatings leading to activation of the complement system, inducing inflammatory responses as well as activation of coagulation.^[8a,14] The next generation of coatings has been based on other polymers with improved ability to organize water, usually based on zwitterionic (meth)acrylic monomers, such as carboxy-, sulfo- and phosphobetaines and more recently on *N*-(2-hydroxypropyl) methacrylamide (HPMA).^[15] Brushes and brush-like coatings from these polymers resulted in a drastic reduction of protein adsorption and activation as well as strong repulsion of platelets and bacteria.^[3d,11a,16] However, none of these coatings stop coagulation once it has started. The second concept, active coatings, relies on different mechanisms to either counteract clot formation by actively intervening in the coagulation cascade or to reverse clot formation by lysis of nascent clots on the surface.^[17] This includes the display or release of inhibitors of coagulation factors and antiplatelet agents, release of nitric oxide and digestion of neutrophil extracellular trap, and display of thrombolytic agents.^[18] In spite of the improved hemocompatibility, passive as well as active coatings fail to completely inhibit surface-induced coagulation. On the one hand, passive antifouling coatings fail as soon as very small amounts of coagulation factors manage to adsorb and self-amplification mechanisms becomes activated resulting in the propagation of coagulation and clot formation.^[9] On the other hand, current active coatings fail, since they do not prevent fouling, thereby their surface is rapidly coated with proteins leading to a loss of activity.^[19] Moreover, they usually do not discriminate between the passive and the active coagulation factors, thus rapidly becoming exhausted.^[20]

But how can blood be safely interfaced with materials? Healthy vascular endothelium is the only truly hemocompatible material as it combines a stealth interface with active mechanisms to modulate and maintain the hemostatic balance.^[21] This has inspired the development of interactive hemocompatible coatings.^[22] These are a class of coatings that are designed to be non-thrombogenic (dormant) yet capable of detecting blood activation switching into an active state to reestablish hemostasis. In this context, we recently developed a fibrinolytic coating that provides a non-thrombogenic interface and is designed to remain in a dormant state but in the presence of thrombi reversibly transitions into an activated state, directing blood's fibrinolytic system to digest the thrombi.^[22] This endows the nanoscopic coating with the ability to direct the digestion of macroscopic clots clearing the surface from the threat. In this work, we introduce a new type of interactive hemocompatible coating that counteracts the root cause of surface-induced coagulation rather than digesting the thrombus after it has been formed. This interactive hemocompatible coating (Figure 1B) controls coagulation locally at two hierarchical levels (passive and active). At the passive level, our coating is designed to render any polymeric surface stealth and non-thrombogenic (antifouling), yet as soon as there is a trace of FXIIa, the coating is capable to immediately capture and block it, thereby switching-off the contact activation and inhibiting amplification reactions and dissemination of coagulation. The passive level of our coating consists of antifouling brushes of HPMA and carboxybetaine methacrylamide (CBMAA)

polymerized by Single Electron Transfer–Living Radical Polymerization (SET-LRP).^[16c] We developed a new strategy to graft these brushes from a wide range of polymer materials, regardless of their chemical nature. The strategy consists of the use of a water-soluble polymer bearing multiple phenylazide and bromoisobutyrate groups. The former provides covalent linkage to the surface of polymer materials^[23] while the latter serves as initiating site for SET-LRP.

The active hierarchical level is introduced by the immobilization of a human anti-FXIIa antibody on the brushes. This antibody selectively inhibits FXIIa by binding to its catalytic site and does not interfere with FXII zymogen or other blood processes related to physiological hemostasis (extrinsic pathway).^[24] Since the activity of our coating is confined to the surface, it is capable of preventing coagulation without affecting overall hemostasis.^[25] We showed that the coating prevented both protein adsorption and bacteria colonization. Simultaneously, the immobilized human anti-FXIIa antibody was active and capable of specifically capturing and inactivating biologically relevant concentrations of FXIIa. Moreover, the active nanocoatings did not show further activation of coagulation nor deposition of clots static in vitro blood contact experiments, thereby proving a new avenue to improve the hemocompatibility of a range of materials.

2. Results and Discussion

2.1. Passive Level – Antifouling Brushes

2.1.1. Synthesis of Macroinitiator

We developed a new type of macroinitiator to address the grafting of brushes from the surface of a wide range of polymeric materials. The macroinitiator is designed to be water-soluble, strongly adsorb at the interface between water and hydrophobic polymers and covalently bind to the latter after UV irradiation, forming an ultra-thin film with initiator groups. The backbone of the macroinitiator consists of a statistic copolymer of *N*-vinylformamide (NVF) and *N*-vinylacetamide (VAm) polymerized by free radical polymerization in isopropanol (Figure S1, Supporting Information).^[26] Subsequently, the formamide groups were partially hydrolyzed to amine groups in aqueous hydrochloride solution yielding a hydrophilic poly(vinylamine-*co*-vinylformamide-*co*-vinylacetamide) copolymer (NVA-*co*-NVF-*co*-VAm) with 44% of free amine groups, 8% residual formamide units and 48% of vinylacetamide units. The molecular weight was $M_n = 3.87 \times 10^3 \text{ g mol}^{-1}$ as determined by size exclusion chromatography with a degree of polymerization of $DP_n = 60$ calculated from NMR analysis (Figures S3 and S4, Supporting Information). The amine groups were utilized to introduce the tetrafluorophenylazide and bromoisobutyrate groups by reacting the polymer with *N*-succinimidyl-4-azido-tetra-fluorobenzoate (PFPA-NHS) and 2-bromoisobutanoic acid *N*-hydroxy-succinimide ester (BIB-NHS, Figure S1, Supporting Information). The resulting macroinitiator (NVA-*co*-NVF-*co*-VAm-*co*-PFPA-*co*-BIB) contained 34.5% and 3.5–5.0% of the repeating units modified with PFPA-adhesion promoting groups and of BIB-initiator groups respectively (¹H-NMR, Figure S5, Supporting Information). The modular synthesis of

the macroinitiator enables to tailor the properties of the final coating. On the one hand, the grafting density can be controlled through the ratio of initiator to adhesion groups and on the other hand, different types of functional monomers can be grafted from the macroinitiator with varying thickness.

2.1.2. Grafting of Antifouling Polymer Brushes

The macroinitiator was utilized to functionalize different materials, namely hollow fiber membranes of PMP, PCL electrospun

scaffolds and PE wound contact layers. Briefly, the substrates were coated by immersing them into a 1 mg mL⁻¹ macroinitiator solution in water. Continuous UV-irradiation for 60 min triggered the formation of nitrene radicals at the PFPA groups, which inserted into C–H bonds of the substrate (Figure 2A) cross-linking the macroinitiator on the surface. This resulted in a layer with a thickness in the range of 1.6–4.1 nm as determined by ellipsometry on model silicon substrates with the corresponding spin-coated polymers (Table S1, Supporting Information). Such ultra-thin layers indicate that the functionalization mechanism only

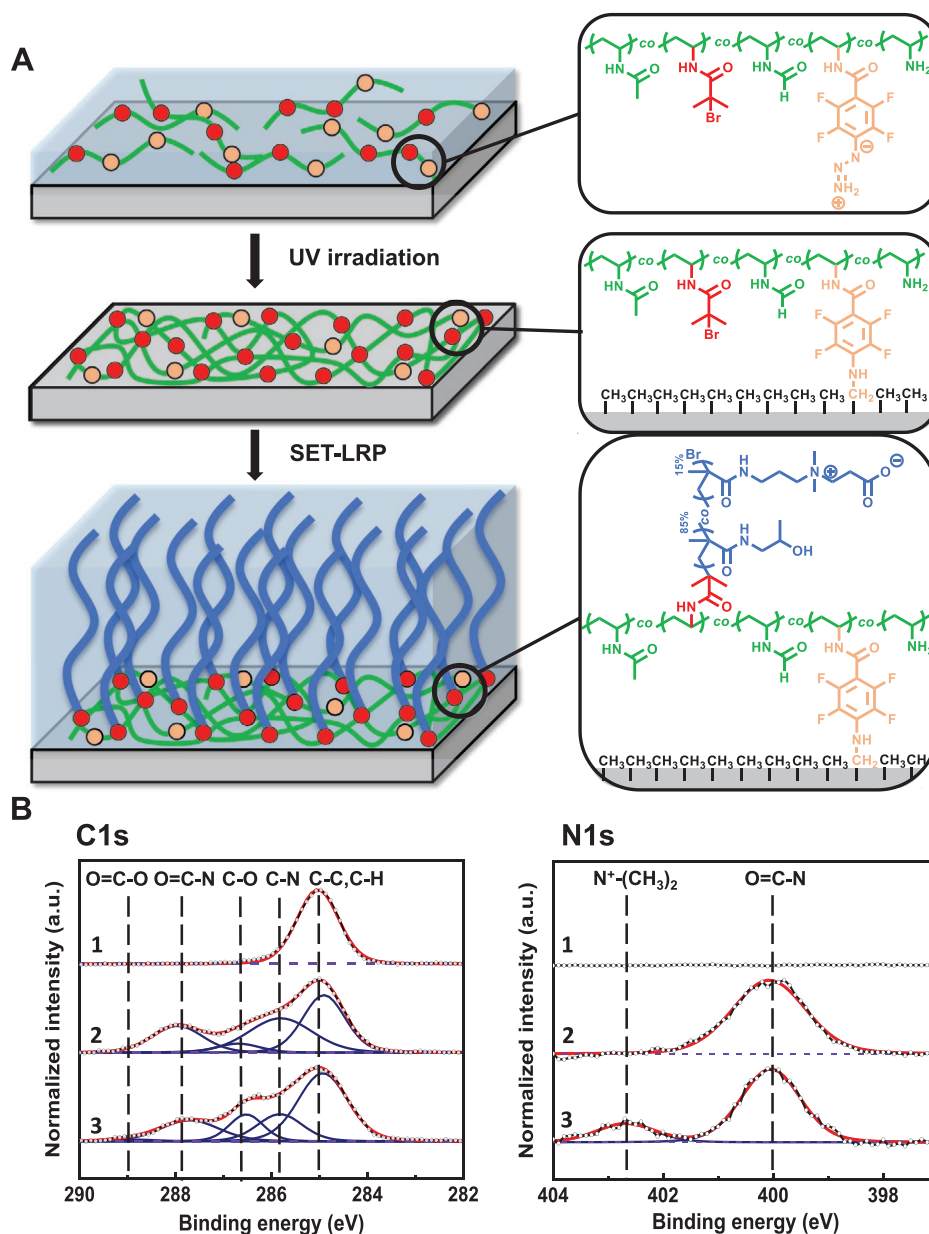


Figure 2. A) Overview of the formation of the antifouling nanocoating on polymeric materials. The macroinitiator dissolved in an aqueous solution adsorbs and spreads onto the polymeric surface. UV-irradiation generates nitrene radicals that insert into C–H crosslinking the macroinitiator to the material's surface. This strategy can be utilized with any organic substrate to introduce initiator groups. Brushes are grafted from the macroinitiator layer by SET-LRP. B) High-resolution XPS spectra C1s (left) and N1s (right) of 1) bare PMP hollow fibers, 2) fibers functionalized with macroinitiator and 3) poly(HPMA-co-CBMAA) brushes grafted from macroinitiator onto hollow fibers.

includes the monomolecular adsorption of chains to form the layer.

Copolymer brushes of HPMA (85%) and CBMAA (15%) were grafted from the coated surfaces by photoinduced SET-LRP in DMSO with traces of copper catalyst (40 ppb) at ambient conditions.^[27] Brushes of 30–40 nm were achieved after 40 min of continuous UV irradiation. The increase in ellipsometric thickness was also accompanied by the disappearance of the F signal in the X-ray photoelectron spectroscopy (XPS) survey spectrum (Figure S14, Supporting Information). Scanning electron microscopy (SEM) images show that the PMP and PCL fiber morphology was not affected by the entire coating procedure (Figure S7, Supporting Information). XPS was utilized to probe the formation of the brushes onto the tested materials (Figure 2B; and Figures S8 and S9, Supporting Information). Figure 2B shows the C1s and N1s spectrum of PMP-hollow fibers for each functionalization step as a representative example. After modification with the macroinitiator a nitrogen peak at 400 eV (from NVA-co-NVF-co-Vam) and a fluorine peak at 688 eV (from PFFA) are visible in the survey spectrum (Figure S8, Supporting Information). Moreover, the C1s high-resolution spectrum shows additional peaks stemming from the [C–N] (285.7 eV) and [O=C–N] (287.7 eV) bonds, which can be assigned to the amine and amide bonds of the macroinitiator. The grafted poly(HPMA-co-CBMAA) brushes can be clearly distinguished by the high-resolution N1s spectrum showing a second nitrogen signal of the quaternary amine [N⁺(CH₃)₂] at 402.6 eV, characteristic for the CBMAA comonomer. Moreover, grafting of poly(HPMA-co-CBMAA) drastically decreased the interfacial tension with water (Table S1, Supporting Information). The non-wettable PMP surface ($\Theta_{adv} = 122.5^\circ$ and $\Theta_{rec} = 99.5^\circ$ with water) could be wetted by water ($\Theta_{adv} = 52.9^\circ$ and $\Theta_{rec} = 28.3^\circ$) after brushes were grafted. These results demonstrate the successful hydrophilization of the surface, minimizing the interfacial energy with water, which is a necessary condition for creating an antifouling surface that prevents the adsorption and unfolding of proteins.^[28]

2.1.3. Repellency to Blood Plasma Proteins

The first step toward a fully hemocompatible surface is to prevent the adsorption and activation of blood proteins on the surface. Conventionally, the adsorption from human serum albumin (HSA) and fibrinogen has been used to study the resistance to fouling. However, repellency against these single-protein solutions does not account for the complex nature of blood. Thus, we assessed the antifouling properties of our coating with undiluted blood plasma using surface plasmon resonance spectroscopy (SPR).

The contact of blood plasma with high surface energy materials, such as gold, leads to very fast adsorption of large amounts of proteins. For example, only five minutes of contact were sufficient to form a full monolayer deposit on gold (270 ng cm⁻², Figure S10B, Supporting Information). In stark contrast, our poly(HPMA-co-CBMAA) brush coating exhibited improved repellency to blood plasma proteins reducing fouling by 91% (23 ng cm⁻²) after 60 min of contact. Thus, the performance of this nanocoating is comparable to the best polymer

brushes directly grafted from self-assembly monolayers of initiators on gold surfaces.^[29] Notably, our nanocoating exhibits superior resistance to fouling compared to the state-of-the-art coatings for blood contacting devices, which can reduce but not prohibit protein adsorption when challenged with less complex single-protein solutions.^[30]

2.1.4. Cytocompatibility of the poly(HPMA-co-CBMAA) Coating

We assessed the cytocompatibility of coated substrates (PMP hollow fiber membrane, PCL nanofiber scaffold, PE wound contact layer, Figure 3A; Figure S11, Supporting Information) by incubating them with human fibroblasts and subsequently

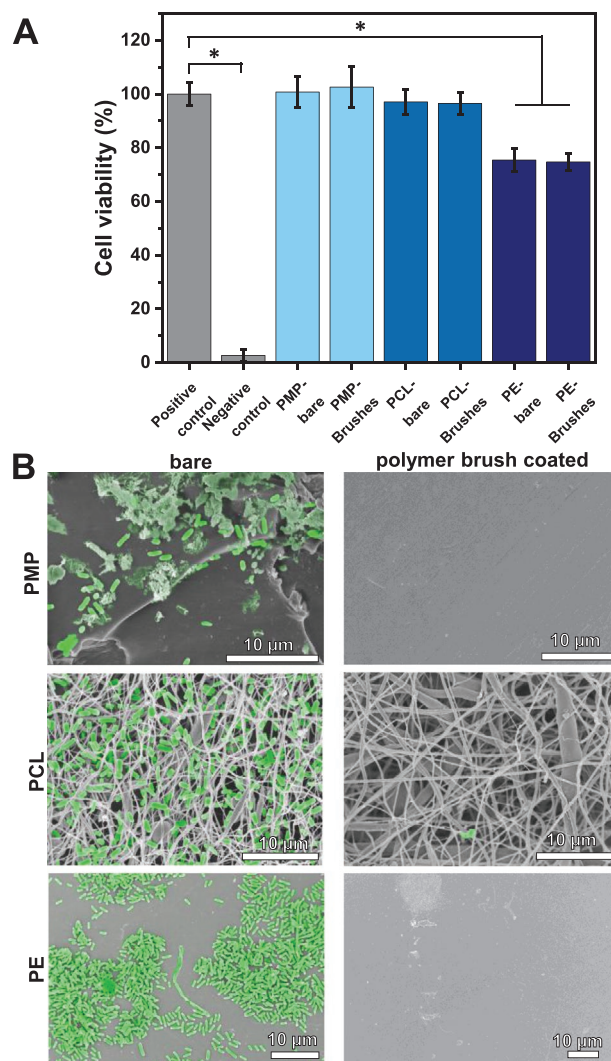


Figure 3. A) Cell viability of normal human dermal fibroblasts determined by MTS assay after 72 h of incubation in direct contact with substrates ($n = 3$, statistical significance for $*p < 0.05$). Untreated cells were set as positive control, while latex gloves serve as negative control. B) Representative SEM micrographs of pristine (left) and coated (right, poly(HPMA-co-CBMAA) brushes) PMP hollow fibers, PCL electrospun scaffolds and PE wound contact layer after incubation with a suspension of *E. coli* (OD₆₀₀ = 0.1) in Lysogeny broth ($n = 3$).

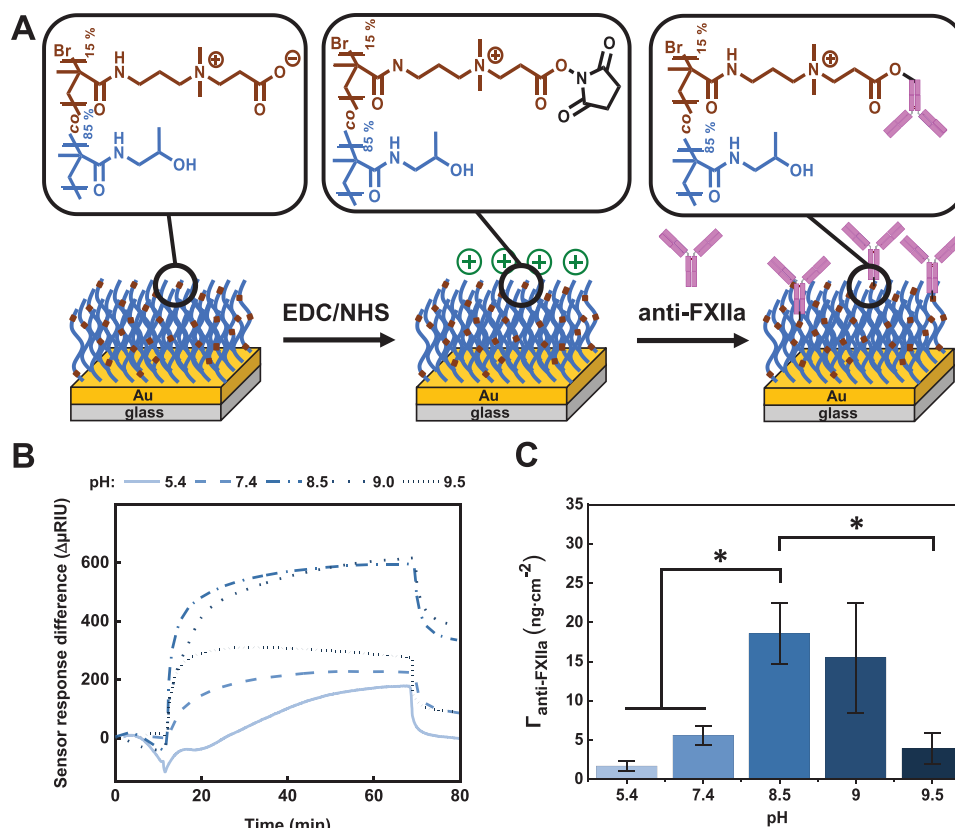


Figure 4. A) Scheme of the functionalization of poly(HPMA-co-CBMAA) brushes with anti-FXIIa depicting the main chemical structures. B) Representative response curves of the anti-FXIIa immobilization recorded at different pHs, C) $\Gamma_{\text{anti-FXIIa}}$ measured at a pH range of 5.4 to 9.5 ($n = 3$, statistical significance for $*p < 0.05$).

determined the metabolic activity of the cells (MTS assay). After incubation for 72 h, all of the studied uncoated materials displayed high cell viability (above 70%). Fibroblasts incubated with PMP and PCL substrates exhibited the same metabolic activity as the positive control (culture plate, above 97%). In the case of PE, the bare material resulted in a reduction in cell viability of 24%, indicating that the uncoated PE substrates used were not completely harmless to the fibroblasts in spite of being a wound contact layer. The coating of these wound contact layers did not cause any further reduction of its compatibility, which always remained above 75% compared to the positive control. Thus PE and the coatings are considered non-cytotoxic. Notably, the application of the macroinitiator and our polymer brush coatings led to no significant changes in the metabolic activity of the cells resulting in equivalent cell viability (at least 99% when compared to the bare substrates) and no cytotoxicity.

2.1.5. Prevention of Bacterial Adhesion

In addition to coagulation, bacterial colonization poses a major threat for blood contacting devices potentiating the risk of complications. *Escherichia coli* is a common pathogen associated with nosocomial infections.^[31] Even a non-pathogenic laboratory strain of these bacteria can rapidly adhere onto PMP, PE flat surfaces as well as electrospun PCL nanofibers. *E. coli* could rapidly cover 22 and 42% of the surface of PMP and PE

respectively and adhered to the intricate fibrous structure of PCL. Moreover, after gaining access to the intricate internal surface of nanofiber meshes or the hollow fiber membranes they were protected from mechanical removal, which enables them to form biofilm (Figure 3B).

On the other hand, the application of the coating had a drastic effect on the ability of bacteria to adhere to these surfaces. Hardly any bacterium could be found on flat PE wound contact layers after coating with poly(HPMA-co-CBMAA) brushes. Remarkably, a similar level of protection was observed for the nanofiber meshes and hollow fibers. In both cases, bacteria could neither adhere onto the surface of exterior nor interior fibers. This means that this facile strategy to produce the coating was capable of growing brushes even inside the intricate mesh of fibers protecting all surfaces, which could be colonized by these microorganisms. Such a strong repulsion is in agreement with extremely low adhesion energies that have been reported for the most antifouling polymer brushes.^[16e,g]

2.2. Active Level – Anti-FXIIa Antibody

2.2.1. Immobilization of Anti-FXIIa on Polymer Brushes

Poly(HPMA-co-CBMAA) brushes were functionalized with a humanized anti-FXIIa antibody that exclusively binds FXIIa. To monitor the binding kinetics we grafted the

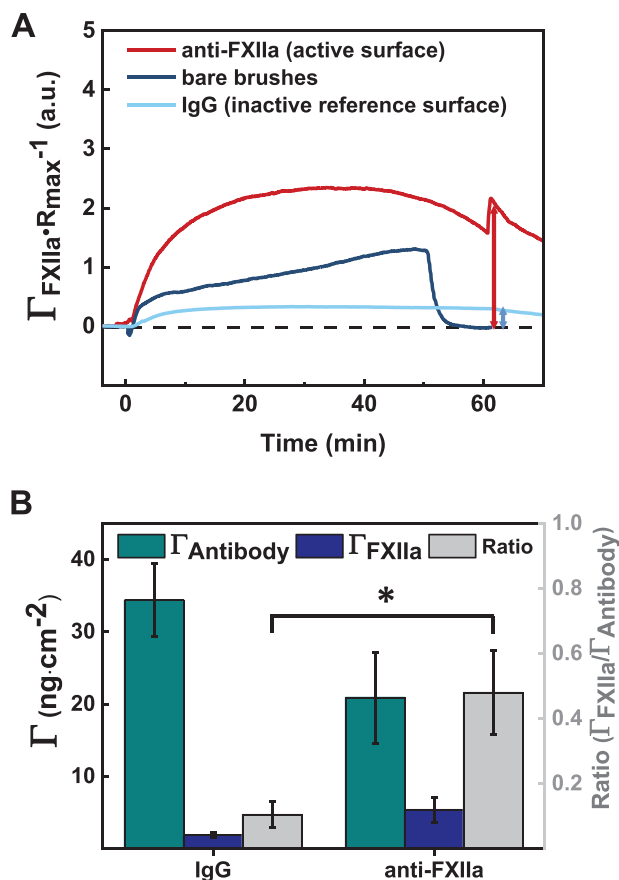


Figure 5. A) Binding kinetics of FXIIa (10 nM) on bare (light blue), IgG- (blue) and anti-FXIIa-functionalized (red) brushes. The response was fitted to R_{max} of the surface. B) Comparison of the amount of immobilized antibody (IgG vs. anti-FXIIa) and the corresponding amount of FXIIa captured on the surface after injection ($\Gamma_{\text{anti-FXIIa}}$: green, Γ_{FXIIa} : blue, ratio: grey, $n = 3$, statistical significance for $*p < 0.05$).

poly(HPMA-*co*-CBMAA) brushes from gold-coated SPR sensor chips and immobilized anti-FXIIa by amine coupling using *N*-(3-dimethylaminopropyl)-*N'*-ethylcarbodiimide hydrochloride (EDC) and *N*-hydroxysuccinimide (NHS) (Figure 4A). EDC and NHS react with the carboxyl groups of the carboxybetaine comonomer to form an active NHS-ester rendering the brush surface positively charged. Any free amine group of the antibody can attack the active esters and covalently bind on top of the brush surface.^[32] To optimize the surface modification, we studied the immobilization kinetics of anti-FXIIa (50 $\mu\text{g mL}^{-1}$) in a pH range from 5.4 to 9.5 in different running buffers (sodium acetate (SA) pH 5.4, phosphate buffered saline (PBS) pH 7.4, sodium borate (SB) pH 8.5, 9.0, 9.5) (Figure 4B,C) by SPR. Increasing the pH resulted in a drastic change in the initial binding rate (steeper sensor response curve) and a stronger sensor response. The density of the immobilized antibody ($\Gamma_{\text{anti-FXIIa}}$) increased until pH 8.5 and decreased thereafter. At pH 8.5 or higher, the antibody is above its isoelectric point (IEP = 8.4), i.e., it is negatively charged. Thus, the increase in $\Gamma_{\text{anti-FXIIa}}$ when the pH is changed from 5.4 to 8.5 is associated with attractive interactions between the positively charged activated brushes and the negatively charged antibody. Over tenfold

more anti-FXIIa was immobilized (18.6 ng cm^{-2}) compared to pH 5.4 (1.7 ng cm^{-2}). Further increasing the pH to 9.5 resulted in similar initial binding rates. However, due to the susceptibility of the formed NHS ester to hydrolysis, rapid surface inactivation occurred, resulting in a reduced sensor response and yielding only low amounts of adsorbed anti-FXIIa (3.9 ng cm^{-2}). Moreover, the immobilization of anti-FXIIa did not have any negative effect on the antifouling performance of the brushes. The contact with blood plasma resulted in a minuscule amount of fouling (4.5 ng cm^{-2} , Figure S12, Supporting Information), which is negligibly higher than the fouling observed on the corresponding non-functionalized poly(HPMA-*co*-CBMAA) brushes (3.3 ng cm^{-2}). This result indicates, first, that FXII is neither captured by anti-FXIIa nor activated at the surface and second, that the structure of the brush is preserved upon immobilization and its excellent protein repellency is maintained.

2.2.2. Specific Capture of FXIIa

We further assessed the activity of the coating to capture FXIIa within biologically relevant concentrations (10 nM, 0.8 $\mu\text{g mL}^{-1}$ in PBS) and determined the binding kinetics by SPR (Figure 5A).^[33] As a control for non-specific binding of FXIIa to the surface, we used bare polymer brushes and polymer brushes functionalized with an immunoglobulin G mixture (IgGs) from human serum. In order to make the IgG-functionalized surfaces comparable, the response curves were fitted to the respective maximum theoretical response capacity (R_{max} value, Supporting Information).^[34] R_{max} is a theoretical estimation of the maximum binding capacity assuming that every immobilized ligand is accessible for analyte binding which allows to compare surfaces with different number of immobilized ligands.^[35] After 60 min contact, the anti-FXIIa-polymer brushes (12.3 ng cm^{-2} anti-FXIIa) captured 6.4 ng cm^{-2} of FXIIa, which corresponds to a molar analyte/ligand ratio of 0.63 (Figure 5B). In stark contrast, no adsorption was detected on the bare polymer brushes and only minute amounts of FXIIa (1.6 ng cm^{-2}) adsorbed on the IgG-polymer brushes (37.9 ng cm^{-2} IgG, analyte/ligand ratio of 0.08). These findings confirmed that the binding of FXIIa by anti-FXIIa proceeds via specific antibody–antigen interactions rather than non-specific protein fouling.

Moreover, to prevent the self-amplification of FXIIa and concomitant activation of coagulation, not only specificity but also high binding affinity and fast binding kinetics are required. In order to estimate the binding affinity of immobilized anti-FXIIa, we recorded the binding kinetics of FXIIa at three different concentrations (10, 50, 100 nM, Figure S13A, Supporting Information) by SPR. The resulting response curves were fitted to a binding model for 1:1 analyte–ligand interactions that account for surface immobilization of the ligand (Figure S13B,C, Supporting Information).^[36] The immobilized anti-FXIIa showed a high binding affinity toward FXIIa in the nanomolar range ($K_{\text{D}} = 6.01 \pm 0.16 \times 10^{-8}$ M), similar to the one previously reported for the antibody.^[22a,32] Thus, the immobilization on the brushes did not impair the activity of antibody toward FXIIa (30–70%, Table S2, Supporting Information).^[37]

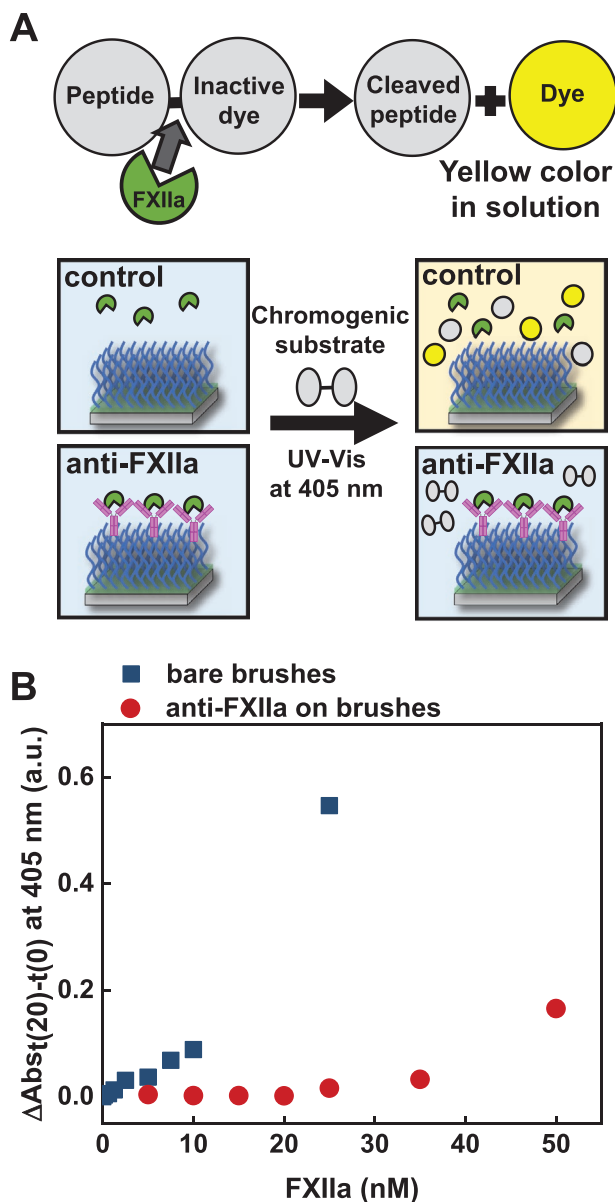


Figure 6. A) Concept of the activity assay of anti-FXIIa functionalized brushes on membrane oxygenator hollow fibers using a chromogenic substrate. B) Plot of $\Delta Abs_{t(20)-t(0)}$ against the initial FXIIa concentration in the analysis solution demonstrating the activity of anti-FXIIa functionalized hollow fibers.

2.2.3. In Vitro Activity of Anti-FXIIa Functionalized Membrane Oxygenator Fibers

The success of the concept relies on the rapid capture of FXIIa before it can promote amplification and further activation. Thus we analyzed the activity of anti-FXIIa immobilized on brushes on PMP-hollow fibers using a chromogenic substrate containing a peptide sequence that can be specifically cleaved by FXIIa (Figure 6A). Cleavage of the peptide releases *p*-nitroaniline, which is detectable by UV–vis spectroscopy (405 nm). We hypothesized that PMP hollow fibers coated with anti-FXIIa functionalized polymer brushes capture FXIIa on

the surface, lowering the overall concentration of FXIIa in solution. Thus, the cleavage of subsequently added chromogenic substrate would be attenuated compared to a starting solution without anti-FXIIa functionalized fibers. To analyze the performance of our interactive coating under practical conditions, we performed the following experiments with a membrane-to-liquid ratio similar to the membrane-to-blood ratio during ECMO treatment (3 L m⁻², 6 L of blood and 2 m² membrane). PMP fibers with the interactive anti-FXIIa nanocoating or bare polymer brushes (control) were incubated in solutions of FXIIa (1 mL, 0.078–50 nM) for 45 min to allow capture of FXIIa. Subsequently, the fibers were removed, the chromogenic substrate was added (CS-31(02), 0.1 mL, 2.3 μM) and the change in absorbance at 405 nm was recorded for 20 min ($Abs_{t(20)}$).

The $\Delta Abs_{t(20)-t(0)}$ value was plotted against the initial concentration of FXIIa in solution (Figure 6B). As expected, the increase of the initial FXIIa concentration in the control led to more cleavage of the chromogenic substrate and greater *p*-nitroaniline release resulting in higher $\Delta Abs_{t(20)-t(0)}$. Conversely, fibers decorated with anti-FXIIa functionalized polymer brushes prohibited the cleavage of the chromogenic substrate up to FXIIa concentrations of 35 nM while thereafter some increase in absorbance was observed. For example, to achieve a reduction in ΔAbs from 0.547 (control) to 0.016 corresponds to [FXIIa] quenching from 25 to 1.5 nM which is equivalent to 94% of free FXIIa. Moreover, only a minor release of *p*-nitroaniline could be observed for [FXIIa] higher than 30 nM after incubation with the fibers decorated with anti-FXIIa. Overall, the interactive anti-FXIIa nanocoating effectively captured biologically relevant concentrations of FXIIa on the surface and allows to actively intervene at the earliest stage of coagulation.^[38]

2.2.4. Interaction of Anti-FXIIa Functionalized Membrane Oxygenator Fibers with Human Blood

To achieve a hemocompatible surface, the anti-FXIIa coating must reject cellular components from blood as well as proteins, since adherent and activated platelets and leukocytes can bypass the contact system and trigger clotting on the surface.^[39] We performed static blood experiments where the substrates (bare PMP membrane, PMP coated with brushes, and brushes functionalized with anti-FXIIa) were incubated in 1 mL of citrated blood at 37 °C for 2 h (Figure 7). Citrate, a chelating anion, was used to retard the activation of coagulation, which would otherwise immediately start after the blood is withdrawn from the donor. The use of citrate does not affect the study of the contact activation and allows for the evaluation of the performance of the coating minimizing the activation of the latter. The microscopic examination by SEM showed that the surfaces of the uncoated PMP (flat and fibers) were largely covered with platelets that lost their spherical shape and spread on the surface with long appendages, indicating activation (Figure 7A,B). Moreover, crosslinked fibrin networks with deposited cells on top and larger aggregates of erythrocytes were also observed. This demonstrates that this widely used material exerts a negative interaction with blood activating the contact system.

A massive difference was obtained when the antifouling coating was applied to the PMP hollow fibers (Figure 7B, brushes). Only a few platelets or leukocytes managed to adhere

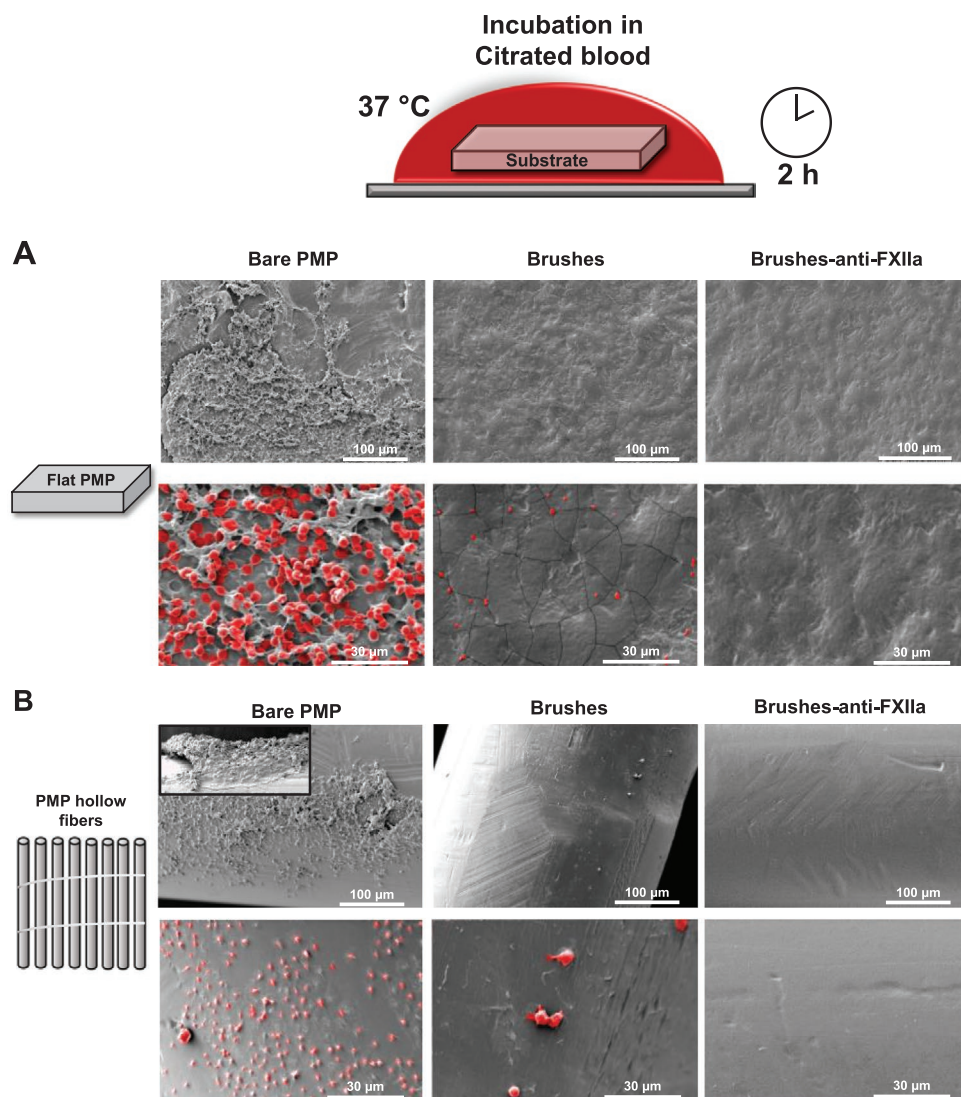


Figure 7. Static blood experiments with citrated human blood at 37 °C for 2 h. SEM images of the fibrin deposition and platelet adhesion on A) flat PMP and on B) PMP-hollow fibers from real human blood after incubation of the fibers for 2 h. First column: bare, unmodified PMP, second column: PMP modified with poly(HPMA-co-CBMAA) brushes, third column: PMP with anti-FXIIa functionalized brushes. The adhered cells are false-colored for improved visualization.

to the surface. Moreover, the interactive anti-FXIIa nanocoating exhibited even better performance by completely preventing the formation of a fibrin network and the adhesion of platelets and cells. This represents a significant improvement in hemocompatibility compared to the bare fibers currently used in real oxygenators in clinical practice. Overall, these results show that our interactive anti-FXIIa nanocoating provides superior protection to prevent clot formation on surfaces.

3. Conclusion

We developed an interactive anti-FXIIa nanocoating for blood-contacting medical devices that synergistically combines a stealth interface against blood protein adsorption with the ability to specifically scavenge activated FXII to tackle the two

root causes of surface-induced coagulation. The coating consists of poly(HPMA-co-CBMAA) brushes functionalized with a humanized anti-FXIIa antibody exerting a total thickness of only 40 nm. By introducing a photoactive macroinitiator we could apply the interactive anti-FXIIa nanocoating onto a broad range of polymers with high medical relevance without the need for harsh pretreatments that otherwise damage the material surface. Coated surfaces exhibited excellent antifouling properties toward proteins from blood plasma, blood cells and *E. coli* bacteria. Moreover, the anti-FXIIa nanocoating captured and inactivated biologically relevant concentrations of FXIIa when applied onto PMP oxygenator membranes showing that immobilized anti-FXIIa preserves its activity and high affinity toward FXIIa. In in vitro static blood experiments the interactive anti-FXIIa nanocoating completely prohibited the formation of clots on the PMP surface. These findings represent enhanced

hemocompatibility of blood contacting devices. The coating not only suppresses the activation of blood proteins but also actively intervenes in the contact activation system and prevents the amplification and propagation of coagulation from the surface.

We envision that our coating strategy can contribute to the next generation of interactive hemocompatible coatings for blood-contacting medical devices. The interactive anti-FXIIa coating can serve as a basis for combination with other blood regulatory factors and functions, such as fibrinolytic agents, which together synergistically mimic the hemostatic regulation exerted by the endothelium and autonomously modulate coagulation.

4. Experimental Section

Materials, Cells and Characterization: Details of materials, fibroblast and bacteria culture, and characterization techniques can be found in the Supporting Information.

UV-Activated Insertion of Macroinitiator on Polymer Substrates: For the coating procedure NVA-co-NVF-co-VAm-co-PFPA-co-BIB was dissolved in Milli-Q-water (1 mg mL^{-1}) and the polymeric substrate was either fully wetted with- or fully immersed into the solution. The substrates were irradiated with UV-light in a self-constructed reactor (144 W, $4 \times 36 \text{ W}$ lamps) for 45–60 min until a color change of the solution from colorless to brownish-yellow was observed. Subsequently, the substrates were thoroughly rinsed with EtOH and Milli-Q-water to remove the unbound crosslinked macroinitiator sticking to the substrate. Afterward, poly(HPMA-co-CBMAA) were grafted from the macroinitiator-coated surfaces by photoinduced SET-LRP.

Standard Protocol for Polymer Brushes Via Photoinduced SET-LRP: A catalyst stock solution (S) was prepared by dissolving CuBr_2 (8.7 mg, $3.9 \text{ } \mu\text{mol}$) and Me_6TREN (62.5 μL , $23.4 \text{ } \mu\text{mol}$) in DMSO (10 mL) and protected from light. In a separate flask, a polymerization solution (P) in DMSO was prepared. One milliliter of solution contained 0.214 g of HPMA (1.49 mmol) and 0.064 g of CBMAA (0.26 mmol). Then, per milliliter of DMSO used, 0.044 mL of (S) were added to (P). The initiator immobilized substrates (wafers, Au-SPR-sensor slides, PMP-hollow fibers) were placed in vials and sealed with a septum. Vials and polymerization solution were degassed by sparging with N_2 for 60 min. Subsequently (P) was transferred to the substrates, which were completely immersed in the solution (wafer: 1 mL, Au-SPR: 1.5 mL, PMP-fibers: 3–4 mL). The polymerization was performed by UV-irradiation with a nail-curing device (Salon Edge, 36 W ($4 \times 9 \text{ W}$ lamps), $\lambda_{\text{max}} = 365 \text{ nm}$) at room temperature. The polymerization was stopped by exposure to air and the addition of 1 mL of DMSO. The substrates were rinsed with EtOH and Milli-Q-water and blow-dried with an N_2 -stream. Au-SPR sensor slides were stored until use in a solution of 95% of Milli-Q-water and 5% of EtOH.

In-Situ Immobilization of Anti-FXIIa on Polymer Brushes by SPR: The immobilization of antibodies to poly(HPMA-co-CBMAA) brushes was followed by SPR to quantify the amount of immobilized antibody. Milli-Q water was flown over the surface until a stable baseline was established. In separate vials, EDC (76.7 mg, 0.49 mmol) and NHS (11.8 mg, 0.10 mmol) were dissolved in 1 mL of Milli-Q-water each. The EDC/NHS solution was freshly prepared by mixing of 0.5 mL EDC- and 0.5 mL of NHS-solution prior to injection. The polymer brush surface was activated by flowing the EDC/NHS solution over the surface for 10 min at a flowrate of $10 \text{ } \mu\text{L min}^{-1}$. After the activation, the surface was flushed with Milli-Q water for 1 min and subsequently switched to the running buffer used for the following immobilization. Then the previously prepared antibody solution ($50 \text{ } \mu\text{g mL}^{-1}$) in 0.1 M running buffer (SB, PBS, SA) was injected for 60 min at a flowrate of $10 \text{ } \mu\text{L min}^{-1}$. Afterward, the surfaces were flushed with PBS for 60 min to hydrolyze residual NHS ester.

Antifouling Measurements: The antifouling properties of 85:15 poly(HPMA-co-CBMAA) brushes with and without immobilized anti-FXIIa were determined using undiluted citrated human blood plasma

(100%). The plasma was flown over the respective surface for 60 min at a flowrate of $10 \text{ } \mu\text{L min}^{-1}$ monitored by SPR to quantify the amount of protein adsorption from blood plasma.

Activity Assessment of Immobilized Anti-FXIIa by SPR: For the activity assessment, anti-FXIIa and IgG from human serum (control) were immobilized on poly(HPMA-co-CBMAA) brushes as described above. After immobilization different concentration of FXIIa in PBS were injected for 60 min at a flowrate of $10 \text{ } \mu\text{L min}^{-1}$ and monitored by SPR-spectroscopy to quantify the amount of captured FXIIa at the surface. In case of consecutive FXIIa injections the surface was regenerated by injection of aqueous hydrochloride solutions ($\text{pH} = 2.5\text{--}3.5$) for 1 min.

Activity Assessment of Immobilized Anti-FXIIa on Hollow Fibers Using a Chromogenic Substrate CS-31(02): Polymer substrates coated with poly(HPMA-co-CBMAA) brushes were immersed in an aqueous solution of EDC/NHS (0.4 M EDC, 0.1 M NHS) for 10 min. Afterward, the substrates were rinsed with sodium borate buffer (0.1 M, $\text{pH} = 8.5$) and directly immersed in a freshly prepared solution of anti-FXIIa or human serum IgG (control surface) in SB buffer ($50 \text{ } \mu\text{g mL}^{-1}$) for 1 h. The substrates were rinsed with SB and PBS and stored in PBS buffer until use. The prepared substrates were incubated for 45 min with PBS solutions spiked with different amounts of FXIIa (0 nm (baseline), 0.078, 0.175, 0.313, 0.625, 1.25, 2.5, 5.0, 7.5, 10, 25 nm). The fibers were separated from the solution and 0.1 mL of CS-3102 (1.25 mg mL^{-1} in Milli-Q water) were added to the solution and well mixed. The mixture was immediately transferred to a UV-vis spectrometer and the change in absorption at 405 nm was measured for 20 min against a neat PBS buffer cell as reference. The data was evaluated by calculation of the difference in the maximal absorption at $t = 20 \text{ min}$ and $t = 0 \text{ min}$. The $\Delta\text{Abs}_{t(20)-t(0)}$ -value was then plotted against the initial concentration of FXIIa in 1 mL of analysis solution (FXIIa+CS-3102 in PBS). To test the activity of the anti-FXIIa functionalized fibers the protocol was performed with anti-FXIIa functionalized fibers.

Static Blood Measurements: Static blood measurements were performed with PMP-hollow fibers with the following modifications: bare, poly(HPMA-co-CBMAA) brushes and anti-FXIIa functionalized poly(HPMA-co-CBMAA) brushes. The blood was collected from 3 healthy donor volunteers (with written consent) and anonymized. A glass slide was used as positive control. One milliliter of citrated blood was added to the PMP-hollow fibers (3 donors per coating type). The surfaces were incubated with blood for 2 h. Afterward, the substrates were removed from blood and rinsed with aqueous NaCl solution for three times. The rinsed substrates were immersed in a 2% glutaraldehyde solution and stored overnight to fix adherent proteins, platelets and cells. The substrates were removed from the glutaraldehyde solution and rinsed with PBS buffer. Water was removed from the substrates by immersing them for 20–30 min in different ethanol solution with ascending concentration (50%, 70%, 85%, 100%). Afterward, the dried substrates were prepared for SEM analysis.

Statistical Analysis: All of the reported experiments were performed at least in duplicates to confirm the reproducibility of the results. All directly measured data are presented without pre-processing unless stated otherwise. Data were expressed as mean \pm standard deviation. All data were processed according to the description in the respective Supporting Information Section. Statistical analysis was determined using Student's t-test in Microsoft Excel 2016. Significant differences were considered at p values < 0.05 ($*p < 0.05$). In Figure 3b representative images for bacteria adhesion on PMP, PE and PCL substrates are shown. Quantification of bacterial surface coverage was performed using ImageJ on the exemplar images. Moreover, Figure 7 shows representative images for blood cell adhesion after contact of whole blood with pristine and coated PMP substrates.

Supporting Information

Supporting Information is available from the Wiley Online Library or from the author.

Acknowledgements

J.Q. and M.G.-S. contributed equally to this work. The authors acknowledge the financial support by the Deutsche Forschungsgemeinschaft (DFG, German Research Foundation) via Schwerpunktprogramm "Towards an Implantable Lung" (Project number: 346972946) and SFB 985 "Functional Microgels and Microgel Systems" (B8), the German Federal Ministry of Education and Research (BMBF) with the project AntiBacCat and Heart2.0 within the "Bio4MatPro-Competence Center for Biological Transformation of Materials Science and Production Engineering" program (grant no. 031B1153A and 031B1154B), and IBEC which is a member of the CERCA Programme/Generalitat de Catalunya. The authors thank Jan Tenbusch for providing the precursor poly(vinylamine-co-vinylformamide-co-vinylacetamide) copolymer (NVA-co-NVF-co-VAM) and its molecular characterization by ¹H-NMR and SEC.

Open access funding enabled and organized by Projekt DEAL.

Conflict of Interest

O.G. has received research funding from Alexsion, Alveron, Bayer, Biotest, Boehringer Ingelheim, CSL Behring, Octapharma, Novo Nordisk, Nycomed, and Werfen. He has also received honoraria for lectures and consultancy support from Baxalta, Bayer AG, Boehringer Ingelheim, Ferring, CSL Behring, Octapharma, Promicul, Pfizer, Takeda, Portola, and Sanofi.

Data Availability Statement

The data that support the findings of this study are available from the corresponding author upon reasonable request.

Keywords

antifouling polymer brushes, anti-FXIIa antibody, factor XII, hemocompatible coatings, interactive hemocompatibility

Received: May 10, 2022

Revised: June 6, 2022

Published online:

- [1] a) B. D. Ratner, *J. Biomed. Mater. Res.* **1993**, 27, 283; b) R. M. Sniecinski, W. L. Chandler, *Anesth. Analg.* **2011**, 113, 1319.
- [2] a) L. Vroman, *Bull. N. Y. Acad. Med.* **1988**, 64, 352; b) L. Vroman, *Colloids Surf., B* **2008**, 62, 1.
- [3] a) L. Vroman, *Materials* **2009**, 2, 1547; b) E. F. Leonard, L. Vroman, *J. Biomater. Sci., Polym. Ed.* **1991**, 3, 95; c) Z. Zhang, M. Zhang, S. Chen, T. A. Horbett, B. D. Ratner, S. Jiang, *Biomaterials* **2008**, 29, 4285; d) X. Lin, K. Wu, Q. Zhou, P. Jain, M. O. Boit, B. Li, H. C. Hung, S. A. Creason, J. Himmelfarb, B. D. Ratner, S. Jiang, *ACS Appl. Mater. Interfaces* **2020**, 12, 41026; e) F. Poncin-Epaillard, T. Vrlinic, D. Debarnot, M. Mozetic, A. Coudreuse, G. Legeay, B. El Moualij, W. Zorzi, *J. Funct. Biomater.* **2012**, 3, 528; f) R. Latour, in *Encyclopedia of Biomaterial Biomedical Engineering*, Francis and Taylor, **2005**.
- [4] a) S. de Maat, C. Maas, *J. Thromb. Haemostasis* **2016**, 14, 1498; b) C. Maas, T. Renné, *Thromb. Res.* **2012**, 129, S73; c) T. Renne, A. H. Schmaier, K. F. Nickel, M. Blomback, C. Maas, *Blood* **2012**, 120, 4296.
- [5] a) C. Maas, C. Oschatz, T. Renné, *Semin. Thromb. Hemostasis* **2011**, 37, 375; b) C. Maas, T. Renne, *Blood* **2018**, 131, 1903.
- [6] a) F. Swieringa, H. M. H. Spronk, J. W. M. Heemskerck, P. E. J. van der Meijden, *Res. Pract. Thromb. Haemostasis* **2018**, 2, 450; b) F. Muller, N. J. Mutch, W. A. Schenk, S. A. Smith, L. Esterl, H. M. Spronk, S. Schmidbauer, W. A. Gahl, J. H. Morrissey, T. Renne, *Cell* **2009**, 139, 1143; c) M. J. Simmonds, N. Watanabe, D. Nandakumar, J. Horobin, in *Mechanical Circulatory and Respiratory Support* (Eds: S. D. Gregory, M. C. Stevens, J. F. Fraser), Academic Press, **2018**, p. 597; d) B. Sivaraman, R. A. Latour, *Biomaterials* **2011**, 32, 5365; e) B. Sivaraman, R. A. Latour, *Biomaterials* **2010**, 31, 832; f) B. Sivaraman, R. A. Latour, *Biomaterials* **2010**, 31, 1036; g) H. Nygren, M. Broberg, *J. Biomater. Sci., Polym. Ed.* **1998**, 9, 817.
- [7] a) J. Janatova, A. K. Cheung, C. J. Parker, *Complement Inflammation* **1991**, 8, 61; b) J. Andersson, K. N. Ekdahl, J. D. Lambris, B. Nilsson, *Biomaterials* **2005**, 26, 1477.
- [8] a) F. Chen, G. Wang, J. I. Griffin, B. Brenneman, N. K. Banda, V. M. Holers, D. S. Backos, L. Wu, S. M. Moghimi, D. Simberg, *Nat. Nanotechnol.* **2017**, 12, 387; b) M. D. Kazatchkine, M. P. Carreno, *Biomaterials* **1988**, 9, 30.
- [9] M. F. Maitz, M. C. L. Martins, N. Grabow, C. Matschegewski, N. Huang, E. L. Chaikof, M. A. Barbosa, C. Werner, C. Sperling, *Acta Biomater.* **2019**, 94, 33.
- [10] a) M. Fischer, M. F. Maitz, C. Werner, in *Hemocompatibility of Biomaterials for Clinical Applications*, (Ed: C. A. Siedlecki), Woodhead Publishing, **2018**, p. 163; b) X. Liu, L. Yuan, D. Li, Z. Tang, Y. Wang, G. Chen, H. Chen, J. L. Brash, *J. Mater. Chem. B* **2014**, 2, 5718.
- [11] a) A. de los Santos Pereira, S. Sheikh, C. Blaszykowski, O. Pop-Georgievski, K. Fedorov, M. Thompson, C. Rodriguez-Emmenegger, *Biomacromolecules* **2016**, 17, 1179; b) L. Li, S. Chen, J. Zheng, B. D. Ratner, S. Jiang, *J. Phys. Chem. B* **2005**, 109, 2934; c) H. Ma, J. Hyun, P. Stiller, A. Chilkoti, *Adv. Mater.* **2004**, 16, 338; d) K. M. Hansson, S. Tosatti, J. Isaksson, J. Wettero, M. Textor, T. L. Lindahl, P. Tengvall, *Biomaterials* **2005**, 26, 861; e) C. K. Pandiyarajan, O. Prucker, B. Zieger, J. Ruhe, *Macromol. Biosci.* **2013**, 13, 873; f) J. K. Meinzer, M. Henze, C. K. Pandiyarajan, O. Prucker, W. Bothe, F. Beyersdorf, J. Ruhe, *ASAIO J.* **2022**, 68, 56; g) E. Brynda, M. Houska, M. Jirouskova, J. E. Dyr, *J. Biomed. Mater. Res.* **2000**, 51, 249; h) R. C. Eberhart, M. S. Munro, J. R. Frautschi, M. Lubin, F. J. Clubb Jr., C. W. Miller, V. I. Sevastianov, *Ann. N. Y. Acad. Sci.* **1987**, 516, 78; i) K. Ishihara, T. Tsuji, T. Kurosaki, N. Nakabayashi, *J. Biomed. Mater. Res.* **1994**, 28, 225.
- [12] a) A. Halperin, *Langmuir* **1999**, 15, 2525; b) A. Halperin, M. Kroger, *Langmuir* **2009**, 25, 11621; c) S. I. Jeon, J. H. Lee, J. D. Andrade, P. G. De Gennes, *J. Colloid Interface Sci.* **1991**, 142, 149; d) L. Leibler, A. Mourran, *MRS Bull.* **1997**, 22, 33.
- [13] a) J. H. Lee, H. B. Lee, J. D. Andrade, *Prog. Polym. Sci.* **1995**, 20, 1043; b) L. D. Unsworth, H. Sheardown, J. L. Brash, *Langmuir* **2005**, 21, 1036; c) L. D. Unsworth, H. Sheardown, J. L. Brash, *Biomaterials* **2005**, 26, 5927; d) D. Leckband, S. Sheth, A. Halperin, *J. Biomater. Sci., Polym. Ed.* **1999**, 10, 1125.
- [14] a) I. Hamad, O. Al-Hanbali, A. C. Hunter, K. J. Rutt, T. L. Andresen, S. M. Moghimi, *ACS Nano* **2010**, 4, 6629; b) T. Riedel, Z. Riedelova-Reicheltova, P. Majek, C. Rodriguez-Emmenegger, M. Houska, J. E. Dyr, E. Brynda, *Langmuir* **2013**, 29, 3388; c) T. Riedel, A. de Los Santos Pereira, J. Taborska, Z. Riedelova, O. Pop-Georgievski, P. Majek, K. Pecankova, C. Rodriguez-Emmenegger, *Macromol. Biosci.* **2022**, 22, e2100460.
- [15] a) Z. Zhang, S. Chen, Y. Chang, S. Jiang, *J. Phys. Chem. B* **2006**, 110, 10799; b) Z. Zhang, T. Chao, S. Chen, S. Jiang, *Langmuir* **2006**, 22, 10072; c) W. Feng, S. Zhu, K. Ishihara, J. L. Brash, *Langmuir* **2005**, 21, 5980; d) N. H. Nguyen, C. Rodriguez-Emmenegger, E. Brynda, Z. Sedlakova, V. Percec, *Polym. Chem.* **2013**, 4, 2424.
- [16] a) G. Cheng, Z. Zhang, S. Chen, J. D. Bryers, S. Jiang, *Biomaterials* **2007**, 28, 4192; b) C. Leng, S. Sun, K. Zhang, S. Jiang, Z. Chen, *Acta Biomater.* **2016**, 40, 6; c) F. Obstals, M. Vorobii, T. Riedel, A. de los Santos Pereira, M. Bruns, S. Singh, C. Rodriguez-Emmenegger, *Macromol. Biosci.* **2018**, 18, 1700359;

- d) C. Rodriguez Emmenegger, E. Brynda, T. Riedel, Z. Sedlakova, M. Houska, A. B. Alles, *Langmuir* **2009**, 25, 6328; e) L. Witzdam, Y. L. Meurer, M. Garay-Sarmiento, M. Vorobii, D. Soder, J. Quandt, T. Haraszti, C. Rodriguez-Emmenegger, *Macromol. Biosci.* **2022**, 22, e2200025; f) M. Garay-Sarmiento, L. Witzdam, M. Vorobii, C. Simons, N. Herrmann, A. de los Santos Pereira, E. Heine, I. El-Awaad, R. Lütticken, F. Jakob, U. Schwaneberg, C. Rodriguez-Emmenegger, *Adv. Funct. Mater.* **2021**, 32, 2106656; g) C. Rodriguez-Emmenegger, S. Janel, A. de los Santos Pereira, M. Bruns, F. Lafont, *Polym. Chem.* **2015**, 6, 5740; h) Y. Liu, D. Zhang, B. Ren, X. Gong, L. Xu, Z. Q. Feng, Y. Chang, Y. He, J. Zheng, *J. Mater. Chem. B* **2020**, 8, 3814.
- [17] a) D. Li, H. Chen, J. L. Brash, *Colloids Surf., B* **2011**, 86, 1; b) D. Li, S. Wang, Z. Wu, H. Chen, J. L. Brash, *Soft Matter* **2013**, 9, 2321; c) D. Li, H. Chen, W. Glenn McClung, J. L. Brash, *Acta Biomater.* **2009**, 5, 1864; d) W. G. McClung, D. L. Clapper, A. B. Anderson, D. E. Babcock, J. L. Brash, *J. Biomed. Mater. Res.* **2003**, 66, 795; e) W. G. McClung, D. E. Babcock, J. L. Brash, *J. Biomed. Mater. Res.* **2007**, 81, 644; f) K. A. Woodhouse, J. L. Brash, *Biomaterials* **1992**, 13, 1103; g) K. Woodhouse, *Biomaterials* **1996**, 17, 75; h) Z. Wu, H. Chen, D. Li, J. L. Brash, *Acta Biomater.* **2011**, 7, 1993; i) H. Du, C. Li, Y. Luan, Q. Liu, W. Yang, Q. Yu, D. Li, J. L. Brash, H. Chen, *Mater. Horiz.* **2016**, 3, 556; j) J. W. Yau, A. R. Stafford, P. Liao, J. C. Fredenburgh, R. Roberts, J. L. Brash, J. I. Weitz, *Acta Biomater.* **2012**, 8, 4092; k) C. Li, H. Du, A. Yang, S. Jiang, Z. Li, D. Li, J. L. Brash, H. Chen, *Adv. Funct. Mater.* **2017**, 27, 1703934; l) W. Zhan, X. Shi, Q. Yu, Z. Lyu, L. Cao, H. Du, Q. Liu, X. Wang, G. Chen, D. Li, J. L. Brash, H. Chen, *Adv. Funct. Mater.* **2015**, 25, 5206.
- [18] a) A. Hosseinnejad, N. Ludwig, A. K. Wienkamp, R. Rimal, C. Bleilevens, R. Rossaint, J. Rossaint, S. Singh, *Biomater. Sci.* **2021**, 10, 85; b) S. Alibeik, S. Zhu, J. W. Yau, J. I. Weitz, J. L. Brash, *J. Biomed. Mater. Res.* **2012**, 100, 856; c) C. Sperling, K. Salchert, U. Streller, C. Werner, *Biomaterials* **2004**, 25, 5101; d) K. E. Kador, T. G. Mamedov, M. Schneider, A. Subramanian, *Acta Biomater.* **2011**, 7, 2508; e) M. F. Maitz, C. Sperling, C. Werner, *J. Biomed. Mater. Res.* **2010**, 94, 905; f) A. Chandiwai, F. S. Zaman, A. E. Mast, C. L. Hall, *J. Biomater. Sci., Polym. Ed.* **2006**, 17, 1025; g) E. Voros, M. Cho, M. Ramirez, A. L. Palange, E. De Rosa, J. Key, Z. Garami, A. B. Lumsden, P. Decuzzi, *Adv. Funct. Mater.* **2015**, 25, 1709; h) M. F. Maitz, J. Zitzmann, J. Hanke, C. Renneberg, M. V. Tsurkan, C. Sperling, U. Freudenberger, C. Werner, *Biomaterials* **2017**, 135, 53; i) Y. Kitamoto, M. Tomita, S. Kiyama, T. Inoue, Y. Yabushita, T. Sato, H. Ryoda, T. Sato, *Thromb. Haemostasis* **1991**, 65, 073; j) G. M. Annich, J. P. Meinhardt, K. A. Mowery, B. A. Ashton, S. I. Merz, R. B. Hirschl, M. E. Meyerhoff, R. H. Bartlett, *Crit. Care Med.* **2000**, 28, 915.
- [19] H. P. Wendel, N. Weber, G. Ziemer, *Immunopharmacology* **1999**, 43, 149.
- [20] B. Tillman, D. Gailani, *Semin. Thromb. Hemostasis* **2018**, 44, 60.
- [21] V. W. van Hinsbergh, *Semin. Immunopathol.* **2012**, 34, 93.
- [22] F. Obstals, L. Witzdam, M. Garay-Sarmiento, N. Y. Kostina, J. Quandt, R. Rossaint, S. Singh, O. Grottko, C. Rodriguez-Emmenegger, *ACS Appl. Mater. Interfaces* **2021**, 13, 11696.
- [23] a) L. H. Liu, M. Yan, *Acc. Chem. Res.* **2010**, 43, 1434; b) L. Liu, M. H. Engelhard, Y. Mingdi, *J. Am. Chem. Soc.* **2006**, 128, 14067; c) M. A. Barlett, M. Yan, *Adv. Mater.* **2001**, 13, 1449; d) Á. Serrano, O. Sterner, S. Mieszkina, S. Zürcher, S. Tosatti, M. E. Callow, J. A. Callow, N. D. Spencer, *Adv. Funct. Mater.* **2013**, 23, 5706.
- [24] a) M. Larsson, V. Rayzman, M. W. Nolte, K. F. Nickel, J. Bjorkqvist, A. Jamsa, M. P. Hardy, M. Fries, S. Schmidbauer, P. Hedenqvist, M. Broome, I. Pragst, G. Dickneite, M. J. Wilson, A. D. Nash, C. Panousis, T. Renne, *Sci. Transl. Med.* **2014**, 6, 222ra17; b) A. H. Schmaier, *Sci. Transl. Med.* **2014**, 6, 222fs7; c) M. Worm, E. C. Kohler, R. Panda, A. Long, L. M. Butler, E. X. Stavrou, K. F. Nickel, T. A. Fuchs, T. Renne, *Ann. Transl. Med.* **2015**, 3, 247; d) Z. Cao, M. Biondo, V. Rayzman, M. Hardy, A. McDonald, S. Busfield, M. W. Nolte, M. Wilson, A. Nash, C. Panousis, *J. Allergy Clin. Immunol.* **2015**, 135.
- [25] J. I. Weitz, J. C. Fredenburgh, *Front. Med.* **2017**, 4, 19.
- [26] K. Yamamoto, T. Serizawa, M. Akashi, *Macromol. Chem. and Phys.* **2003**, 204, 1027.
- [27] a) A. Anastasaki, V. Nikolaou, Q. Zhang, J. Burns, S. R. Samanta, C. Waldron, A. J. Haddleton, R. McHale, D. Fox, V. Percec, P. Wilson, D. M. Haddleton, *J. Am. Chem. Soc.* **2014**, 136, 1141; b) J. Laun, M. Vorobii, A. de los Santos Pereira, O. Pop-Georgievski, V. Trouillet, A. Welle, C. Barner-Kowollik, C. Rodriguez-Emmenegger, T. Junkers, *Macromol. Rapid Commun.* **2015**, 36, 1681; c) M. Vorobii, A. de los Santos Pereira, O. Pop-Georgievski, N. Y. Kostina, C. Rodriguez-Emmenegger, V. Percec, *Polym. Chem.* **2015**, 6, 4210.
- [28] B. Lopez-Mila, P. Alves, T. Riedel, B. Dittrich, F. Mergulhão, C. Rodriguez-Emmenegger, *Bioinspir. Biomim.* **2018**, 13, 065001.
- [29] a) C. Rodriguez-Emmenegger, E. Brynda, T. Riedel, M. Houska, V. Subr, A. B. Alles, E. Hasan, J. E. Gautrot, W. T. Huck, *Macromol. Rapid. Commun.* **2011**, 32, 952; b) J. Ladd, Z. Zhang, S. Chen, J. C. Hower, S. Jiang, *Biomacromolecules* **2008**, 9, 1357.
- [30] a) B. McVerry, A. Polasko, E. Rao, R. Haghniaz, D. Chen, N. He, P. Ramos, J. Hayashi, P. Curson, C. Y. Wu, P. Bandaru, M. Anderson, B. Bui, A. Sayegh, S. Mahendra, D. D. Carlo, E. Kreydin, A. Khademhosseini, A. Sheikhi, R. B. Kaner, *Adv. Mater.* **2022**, 34, 2200254; b) K. Futamura, R. Matsuno, T. Konno, M. Takai, K. Ishihara, *Langmuir* **2008**, 24, 10340; c) S. Kim, S. H. Ye, A. Adamo, R. A. Orizondo, J. Jo, S. K. Cho, W. R. Wagner, *J. Mater. Chem. B* **2020**, 8, 8305.
- [31] S. A. Ferry, S. E. Holm, H. Stenlund, R. Lundholm, T. J. Mønsen, *Scand. J. Infect. Dis.* **2004**, 36, 296.
- [32] a) T. Riedel, S. Hageneder, F. Surman, O. Pop-Georgievski, C. Noehammer, M. Hofner, E. Brynda, C. Rodriguez-Emmenegger, J. Dostálek, *Anal. Chem.* **2017**, 89, 2972; b) T. Riedel, F. Surman, S. Hageneder, O. Pop-Georgievski, C. Noehammer, M. Hofner, E. Brynda, C. Rodriguez-Emmenegger, J. Dostálek, *Biosens. Bioelectron.* **2016**, 85, 272; c) D. Kotlarek, M. Vorobii, W. Ogieglo, W. Knoll, C. Rodriguez-Emmenegger, J. Dostalek, *ACS Sens.* **2019**, 4, 2109.
- [33] S. D. Revak, C. G. Cochrane, A. R. Johnston, T. E. Hugli, *J. Clin. Invest.* **1974**, 54, 619.
- [34] R. L. Rich, D. G. Myszkowski, *J. Mol. Recognit.* **2008**, 21, 355.
- [35] R. Karlsson, A. Michaelsson, L. Mattsson, *J. Immunol. Methods* **1991**, 145, 229.
- [36] S. D. Kramer, J. Wohrle, C. Rath, G. Roth, *Bioinform. Biol. Insights* **2019**, 13, 1177932218821383.
- [37] H. Y. Song, X. Zhou, J. Hogley, X. Su, *Langmuir* **2012**, 28, 997.
- [38] N. V. Zakharaeva, E. O. Artemenko, N. A. Podoplelova, A. N. Sveshnikova, I. A. Demina, F. I. Ataullakhanov, M. A. Panteleev, *PLoS One* **2015**, 10, e0116665.
- [39] M. B. Gorbet, M. V. Sefton, *Biomaterials* **2004**, 25, 5681.